

## Micro-electro-mechanically switchable near infrared complementary metamaterial absorber

Prakash Pitchappa, Chong Pei Ho, Piotr Kropelnicki, Navab Singh, Dim-Lee Kwong, and Chengkuo Lee

Citation: *Applied Physics Letters* **104**, 201114 (2014); doi: 10.1063/1.4879284

View online: <http://dx.doi.org/10.1063/1.4879284>

View Table of Contents: <http://scitation.aip.org/content/aip/journal/apl/104/20?ver=pdfcov>

Published by the [AIP Publishing](#)

---

### Articles you may be interested in

[Dual band complementary metamaterial absorber in near infrared region](#)

*J. Appl. Phys.* **115**, 193109 (2014); 10.1063/1.4878459

[Complementary chiral metasurface with strong broadband optical activity and enhanced transmission](#)

*Appl. Phys. Lett.* **104**, 011108 (2014); 10.1063/1.4861422

[Tunable metamaterials based on voltage controlled strong coupling](#)

*Appl. Phys. Lett.* **103**, 263116 (2013); 10.1063/1.4859636

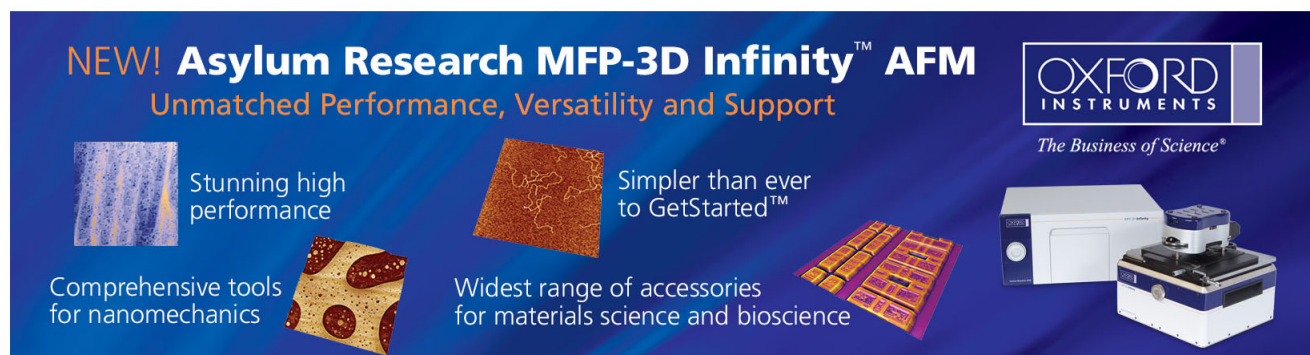
[Triple-band polarization-insensitive wide-angle ultra-thin planar spiral metamaterial absorber](#)

*J. Appl. Phys.* **113**, 213516 (2013); 10.1063/1.4809655

[Nanoimprinted strain-controlled elastomeric gratings for optical wavelength tuning](#)

*Appl. Phys. Lett.* **86**, 161113 (2005); 10.1063/1.1900923

---

The advertisement features a dark blue background with white and orange text. At the top left, it reads 'NEW! Asylum Research MFP-3D Infinity™ AFM' in large white letters, followed by 'Unmatched Performance, Versatility and Support' in orange. On the right, the Oxford Instruments logo is shown with the tagline 'The Business of Science®'. Below the text are several images: a textured surface, a grid of small samples, and the AFM instrument itself. Text boxes describe the instrument's capabilities: 'Stunning high performance', 'Simpler than ever to GetStarted™', 'Comprehensive tools for nanomechanics', and 'Widest range of accessories for materials science and bioscience'.

## Micro-electro-mechanically switchable near infrared complementary metamaterial absorber

Prakash Pitchappa,<sup>1,2</sup> Chong Pei Ho,<sup>1,2</sup> Piotr Kropelnicki,<sup>2,a)</sup> Navab Singh,<sup>2</sup> Dim-Lee Kwong,<sup>2</sup> and Chengkuo Lee<sup>1,b)</sup>

<sup>1</sup>Department of Electrical and Computer Engineering, National University of Singapore, 4 Engineering Drive 3, Singapore 117576

<sup>2</sup>Institute of Microelectronics (IME), 11 Science Park Road, Singapore 117685

(Received 14 April 2014; accepted 11 May 2014; published online 22 May 2014)

We experimentally demonstrate a micro-electro-mechanically switchable near infrared complementary metamaterial absorber by integrating the metamaterial layer to be the out of plane movable microactuator. The metamaterial layer is electrostatically actuated by applying voltage across the suspended complementary metamaterial layer and the stationary bottom metallic reflector. Thus, the effective spacing between the metamaterial layer and bottom metal reflector is varied as a function of applied voltage. With the reduction of effective spacing between the metamaterial and reflector layers, a strong spectral blue shift in the peak absorption wavelength can be achieved. With spacing change of 300 nm, the spectral shift of 0.7  $\mu\text{m}$  in peak absorption wavelength was obtained for near infrared spectral region. The electro-optic switching performance of the device was characterized, and a striking switching contrast of 1500% was achieved at 2.1  $\mu\text{m}$ . The reported micro-electro-mechanically tunable complementary metamaterial absorber device can potentially enable a wide range of high performance electro-optical devices, such as continuously tunable filters, modulators, and electro-optic switches that form the key components to facilitate future photonic circuit applications. © 2014 AIP Publishing LLC. [<http://dx.doi.org/10.1063/1.4879284>]

Electromagnetic (EM) metamaterial is an array of sub-wavelength structures engineered to achieve material properties that are not readily available in nature.<sup>1</sup> This provides a wide range of exciting applications such as invisibility cloaking,<sup>2,3</sup> sub-diffraction imaging,<sup>4,5</sup> and perfect electromagnetic absorbers.<sup>6–10</sup> The metamaterial absorber has become popular, since its first report by Landy *et al.* in 2008; as the proposed absorber was extremely thin and provided design flexibility to achieve near perfect absorption at any desired frequency.<sup>6</sup> Similar absorber designs were then reported over the wide range of electromagnetic spectrum from microwave,<sup>6</sup> terahertz (THz),<sup>7</sup> infrared (IR)<sup>8</sup> to visible frequencies.<sup>9</sup> More recently, tunable metamaterial absorbers have been explored, which enable the absorption characteristics of the devices to be actively controlled through external stimulus.<sup>11–16</sup> Most of these tuning mechanisms are achieved by changing the material properties in terms of either the surrounding medium or the structural layers of devices; through optical,<sup>11</sup> electrical,<sup>12,13</sup> magnetic,<sup>14</sup> thermal,<sup>15</sup> or mechanical<sup>16</sup> means. These approaches either use exotic materials or adopt complex fabrication processes and demand bulky setup for providing external control. Additionally, fabrication process and materials deployed in these active metamaterials is not complementary metal oxide semiconductor (CMOS) compatible and impose a serious hindrance for the application of these tunable metamaterial absorbers into practical devices such as modulators,

multicolor infrared detectors using single pixel, thermal imagers, and electro-optic switch.

In recent years, micro-electro-mechanical system (MEMS) based tunable metamaterial has been reported as a promising candidate to achieve active tuning in metamaterial devices for practical applications. MEMS tunable metamaterial has a whole range of advantages, such as improved tuning range, easier integration with integrated circuit (IC), smaller footprint, faster response, and can be fabricated using CMOS compatible processes. MEMS tunable metamaterial combines the externally controllable microactuators as the metamaterial resonator and the tunability in resonant frequency are achieved by changing the physical pattern shape of the metamaterial unit cell. This is very exciting because the metamaterial as such is designed to have EM properties based on pattern structures rather than the material composition. Hence, MEMS tunable metamaterials demonstrate tunability by reconfiguring the unit cell pattern structures, unlike the earlier tuning schemes that rely on material properties changes with external stimulus.<sup>11–16</sup> Various MEMS tunable metamaterials have been reported by combining different types of microactuators as a part of the metamaterial unit cell, such as out of plane actuated bimorph beams,<sup>17,18</sup> in plane movable comb drives,<sup>19,20</sup> out of plane movable prestressed cantilevers,<sup>21–26</sup> and laterally movable beams.<sup>27</sup> Even though, these reported MEMS tunable metamaterials are very attractive for tunable filter applications, they are not suitable for the design of tunable absorbers in IR spectral region. The disadvantage of the out of plane movable prestressed cantilevers for THz region will have very small initial deformation due to residual stress, owing to reduced pattern size for IR metamaterial. On the other hand, in plane

<sup>a)</sup>Present address: Excelitas Technologies, 8 Tractor Road, Singapore 627969.

<sup>b)</sup>Author to whom correspondence should be addressed. Electronic mail: [elelc@nus.edu.sg](mailto:elelc@nus.edu.sg)

electrostatically actuated MEMS tunable metamaterial suffers from residual stress that can adversely affect the device performance. The in-plane electrostatic comb drive actuator occupies large footprint and the fabrication process will become very complex. Furthermore, actuation voltage and tuning range of the MEMS tunable metamaterial is a design trade off which is a grand challenge in IR region, because of the scaled down unit cell size, i.e., sub-micrometer scale.

In this Letter, we report a MEMS switchable complementary metamaterial absorber (MSCMA) for near-IR spectral region by actively changing the effective spacing formed between the suspended complementary metamaterial (CMM) layer and the fixed bottom metal reflector layer, instead of changing the metamaterial pattern shape as in earlier MEMS tunable metamaterial approaches. We have provided a systematic study of absorption due cavity resonance and the MEMS actuation mechanism that ideally suits for the tunable IR absorber devices. Recently, it was shown that perfect absorption using metamaterial can be explained through interference of electromagnetic waves reflected from the interface of metamaterial and air, and the bottom metal reflector of the metamaterial absorber structure.<sup>25</sup> The key design parameters that determine the peak absorption wavelength are the metamaterial pattern shape and spacer thickness between the metamaterial layer and bottom reflector. The metamaterial pattern shape primarily provides an impedance matching condition, while the spacer thickness defines the cavity resonant condition and hence the peak absorption wavelength. Hence, we leverage the possibility of

changing the effective spacing to actively tune the peak absorption wavelength. The proposed tunability approach using MSCMA enables simpler design, better electro-optic performance, easier integration with control circuitry, smaller device footprint, CMOS compatible materials, and fabrication.

The MSCMA consists of a continuous 200 nm (bm) thick bottom molybdenum (Mo) reflector with a silicon-dioxide ( $\text{SiO}_2$ ) dielectric layer coated with a 40 nm thick aluminum oxide ( $\text{Al}_2\text{O}_3$ ), prepared on a silicon substrate. The  $\text{Al}_2\text{O}_3$  acts as the etch stop layer during vapor hydrofluoric acid release step. The top 100 nm (tm) thick Mo-metal layer is deposited on  $\text{SiO}_2$  sacrificial layer, and becomes a suspended CMM metal membrane after the sacrificial-layer-release step. The schematics of the MSCMA device, unit cell, and fabricated device are as shown in Figs. 1(a)–1(c), respectively. The top CMM membrane with area of  $300 \mu\text{m} \times 300 \mu\text{m}$  consists of rounded-cross air holes as CMM metamaterial patterns. The CMM unit cell has a pitch ( $p$ ) of  $2.515 \mu\text{m}$  along  $x$ - and  $y$ -directions, length ( $l$ ) of  $1.55 \mu\text{m}$  and width ( $w$ ) of  $1 \mu\text{m}$  as shown in Fig. 1(b). The CMM layer is suspended over the  $\text{Al}_2\text{O}_3$  with an air gap,  $g$ . The spacer layer is effectively the combination of three dielectric layers—silicon dioxide ( $\text{SiO}_2$ ), aluminum oxide ( $\text{Al}_2\text{O}_3$ ), and air. The effective spacer thickness,  $d_{EST}$  is determined as  $(n_{\text{SiO}_2} \cdot d_{\text{SiO}_2} + n_{\text{Al}_2\text{O}_3} \cdot d_{\text{Al}_2\text{O}_3} + n_{\text{air}} \cdot g)$ , where  $n_{\text{SiO}_2} = 1.45$ ,  $n_{\text{Al}_2\text{O}_3} = 1.6$ , and  $n_{\text{air}} = 1$  are the refractive index and  $d_{\text{SiO}_2}$ ,  $d_{\text{Al}_2\text{O}_3}$ , and  $g$  are the thickness of  $\text{SiO}_2$ ,  $\text{Al}_2\text{O}_3$ , and air layers, respectively.<sup>29</sup> Now by varying the air gap,  $g$  the effective

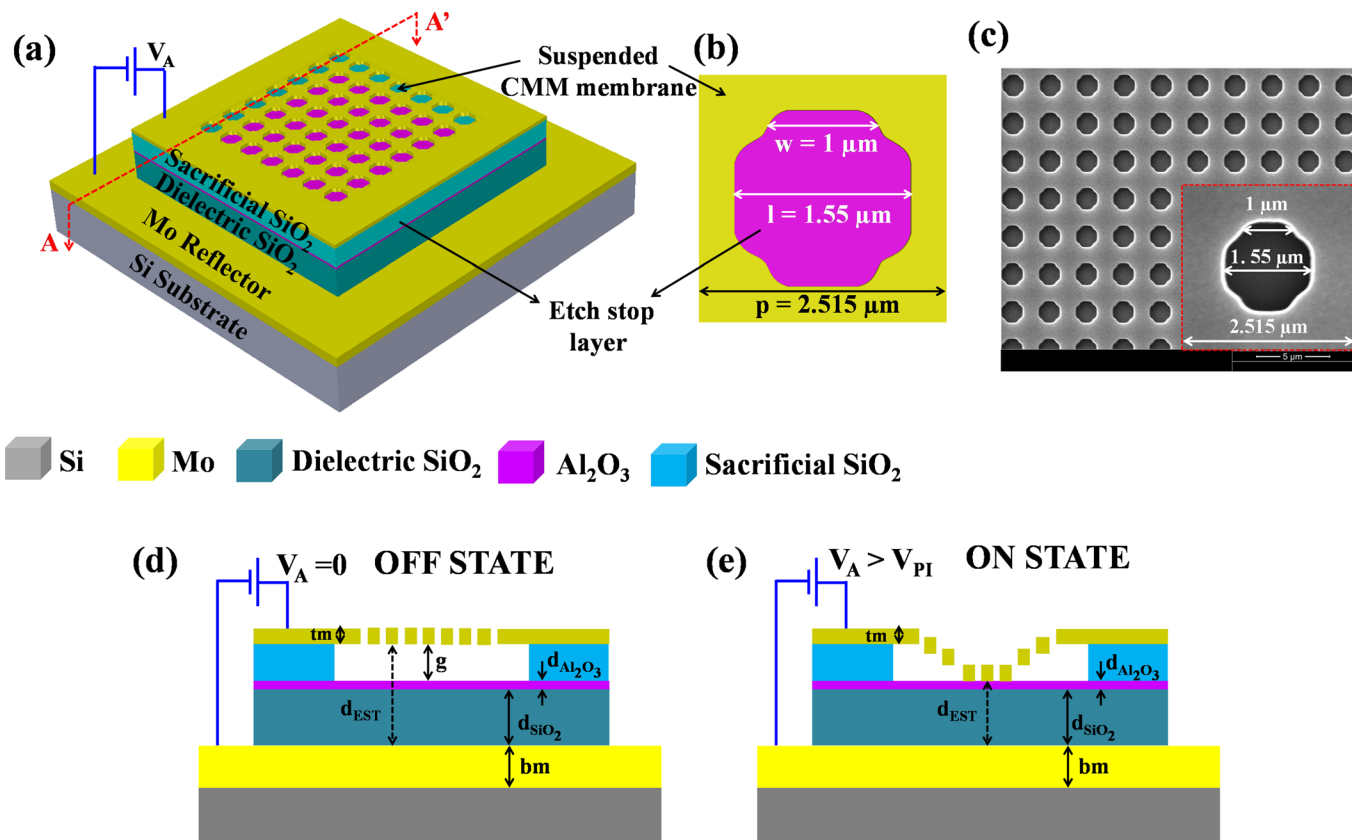


FIG. 1. (a) Schematic of near-IR MEMS switchable complementary metamaterial absorber (MSCMA). (b) Schematic top view of the unit cell with the metamaterial geometry definitions. (c) SEM image of the fabricated MSCMA with the inset showing the unit cell definition. (d) and (e) show the schematic cross sectional view along AA' of MSCMA in OFF state and ON state, respectively.

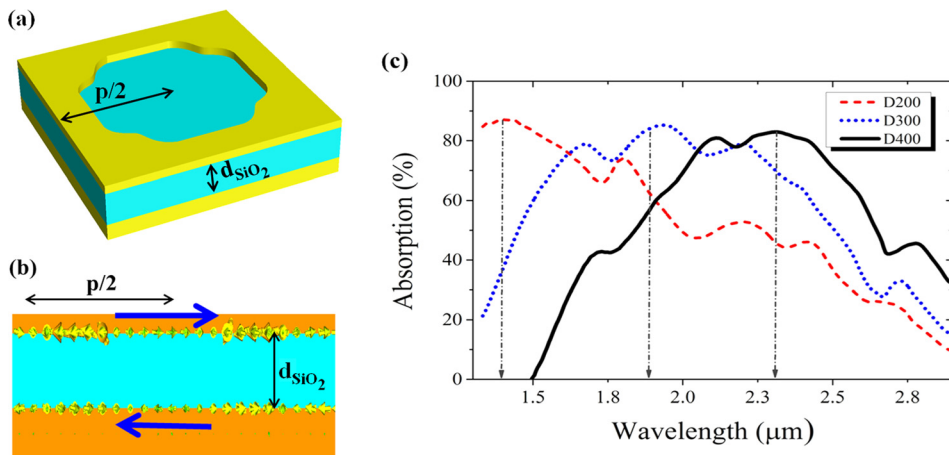


FIG. 2. (a) Schematic drawing of MSCMA unit cell with only SiO<sub>2</sub> as spacer layer, (b) simulated current density for the device shown in (a)  $d_{\text{SiO}_2} = 300$  nm, and (c) measured absorption spectra of devices shown in (a) with varying SiO<sub>2</sub> thickness ( $d_{\text{SiO}_2}$ ): 200 nm for D200 (Red-dash), 300 nm for D300 (Blue-dot), and 400 nm for D400 (Black solid), respectively.

spacer thickness,  $d_{\text{EST}}$  can be changed accordingly. Since the top CMM layer is a continuous sheet of metal, it is used as the movable electrode. When the voltage ( $V_A$ ) is applied across the two metal layers—the suspended CMM membrane and the stationary bottom reflector, the movable CMM membrane will be electrostatically attracted towards the bottom Mo electrode, thereby reducing the air gap,  $g$  which will effectively decrease  $d_{\text{EST}}$ . If the actuation voltage is further increased, the electrostatic force increases as square of decreasing air gap, while the restoring spring force increases almost linearly. Thus, after a critical value of actuation voltage called the pull-in voltage ( $V_{PI}$ ), the electrostatic force overcomes the restoring spring force and causes the top movable CMM layer to come in physical contact with the Al<sub>2</sub>O<sub>3</sub> layer and at this point, there is no more air gap between them, i.e.,  $g = 0$ . For simplicity, we have considered the state, when there is no voltage applied ( $V_A = 0$  V) as OFF state and when voltage,  $V_A > V_{PI}$  is applied as ON State ( $g = 0$ ) as shown in Figs. 1(d) and 1(e), respectively. So as the applied voltage,  $V_A$  increases, the effective cavity thickness,  $d_{\text{EST}}$  decreases and the peak absorption wavelength due to cavity resonance will be shifted to lower wavelength.

In order to elucidate the effect of peak absorption due to cavity resonance with spacer thickness variation, three MSCMA devices were fabricated with different SiO<sub>2</sub> dielectric spacer thickness,  $d_{\text{SiO}_2} = 200, 300,$  and  $400$  nm. For these devices, there was no Al<sub>2</sub>O<sub>3</sub> layer or air gap, i.e.,  $d_{\text{Al}_2\text{O}_3} = g = 0$ . These devices are termed as D200, D300, and D400, respectively. The schematic of these devices is shown in Fig. 2(a). All the devices were measured using an IR microspectrophotometer for the spectral region of  $1.3\text{--}3$   $\mu\text{m}$  with  $45^\circ$  incident angle.<sup>30</sup> The measured absorption spectra for the three devices (D200, D300, and D400) are shown in Fig. 2(c), and it can be observed that with increase in effective spacer thickness,  $d_{\text{EST}}$  ( $= n_{\text{SiO}_2} \cdot d_{\text{SiO}_2}$ ) of  $0.29$   $\mu\text{m}$ , the peak absorption wavelength shows a redshift from  $1.3$  to  $1.92$   $\mu\text{m}$ . Even though the red-shift of the peak absorption wavelength with increasing  $d_{\text{EST}}$  is in accordance to the interference theory,<sup>28</sup> finite-difference time-domain (FDTD) simulations were performed to further understand the resonant mechanism involved. As in the case of the experiments, the excitation source was incident at  $45^\circ$  with electric field along  $x$ -direction for the FDTD simulation. The permittivity of bulk Mo in the near-IR spectral region was

described by the Drude model with the plasma frequency,  $\omega_p = 2\pi \times 1.81 \times 10^{15}$  rad s<sup>-1</sup> and the damping constant,  $\omega_c = 1.24 \times 10^{13}$  s<sup>-1</sup>.<sup>31</sup> The scattering parameters were simulated and the reflection coefficient was then calculated as  $R(\lambda) = |S_{11}(\lambda)|^2$ . The simulated current density for the meta-material absorber, D300 at  $1.92$   $\mu\text{m}$  is shown in Fig. 2(b). The rounded edges of the CMM patterns were also considered in the simulation model using blend edges option in the simulation software. It can be clearly seen that at resonant wavelength, the antiparallel current configuration in the top and bottom Mo layers strongly suggests the cavity mode resonance.<sup>32</sup>

In order to achieve near-IR tunable absorber, three MSCMA devices with different air gaps,  $g = 0$  nm (S\_Ref),  $g = 100$  nm (A100\_OFF), and  $g = 300$  nm (A300\_OFF) were fabricated. The measured IR absorption spectra for these three devices are shown in Fig. 3. The peak absorption wavelength for the reference device S\_Ref, A100\_OFF, and A300\_OFF are around  $2$   $\mu\text{m}$ ,  $2.1$   $\mu\text{m}$ , and  $2.7$   $\mu\text{m}$ , respectively. From Fig. 3, it can be clearly seen that, the peak absorption wavelength increases to higher wavelength with increase in effective thickness of spacer layer,  $d_{\text{EST}}$ . In order to actively control the peak absorption wavelength, an input voltage ( $V_A = 10$  V) was applied across the suspended top CMM Mo membrane and the bottom Mo reflector of

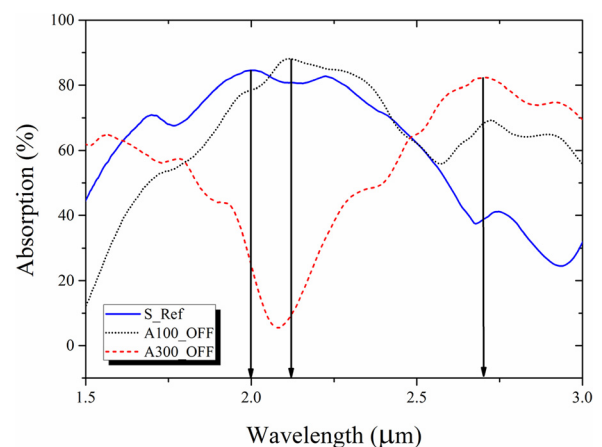


FIG. 3. Measured absorption spectra of MSCMA with different air gaps. No air gap—S\_Ref (Blue-solid), 100 nm air gap—A100\_OFF (Black-dot), and 300 nm air gap—A300\_OFF (Red-dash), respectively.

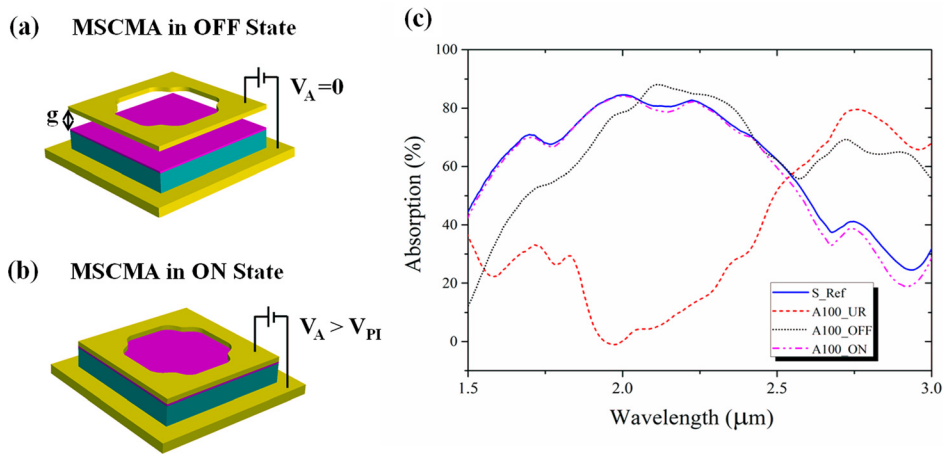


FIG. 4. Schematic drawing of (a) released MSCMA in OFF STATE (before actuation voltage is applied,  $V_A = 0$  V) and (b) released MSCMA in ON STATE (after actuation voltage is applied,  $V_A > V_{PI}$ ). (c) Measured absorption spectra of S\_Ref (Blue-Solid), A100\_UR (Red-dash), A100\_OFF (Black-dot), and A100\_ON (Magenta-dash dot dot) MSCMAs, respectively.

A100\_OFF device. As the input voltage was higher than the  $V_{PI}$  of the device, the top CMM layer comes in contact with the  $Al_2O_3$  layer. The schematics of MSCMA unit cell before and after the applying voltage ( $V_A > V_{PI}$ ) are shown in Figs. 4(a) and 4(b), respectively. The measured IR absorption spectra for devices A100\_OFF ( $V_A = 0$  V) and A100\_ON ( $V_A > V_{PI}$ ) are shown in Fig. 4(c). It can be observed that the effective cavity thickness reduces due to bias voltage, thereby making the peak absorption wavelength to blue shift. Additionally, the absorption spectra of A100\_ON and S\_Ref devices exactly coincide, confirming the absence of air gap after actuation. Even though these MSCMA devices show the possibility of achieving continuously tunable absorber, the experiments could not be carried out at different voltages. This was because the released membrane does not remain flat at intermediate voltages and shows a maximum deflection at center and then gradually reduces towards edges of the membrane. This effect is caused due to the differential spring contact of the all side anchored membrane type actuators. So here, we have characterized the proof-of-concept devices to be potentially used as tunable absorbers using out-of-plane actuated metamaterial layer as an electro-optic switch. So, for the current MSCMA devices, two discrete states are considered—one as released (OFF state) and other completely actuated (ON state). In both the cases, the released CMM membrane remains parallel to the bottom Mo reflector layer.

The electro-optic switching performance of the fabricated MSCMA devices was experimentally studied. The electro-optic switches is very attractive for wide range of applications including data storage,<sup>33</sup> optical switches for telecommunication networks,<sup>34</sup> and multiple gas sensing applications. The two most important performance parameters for the electro-optic switches are higher switching contrast and lower actuation voltage. In order to characterize the proposed MSCMA as an electro-optic switch, a device with 300 nm air gap was fabricated (A300\_OFF). The IR absorption spectra were measured for devices, before (A300\_OFF) and after (A300\_ON) applying voltage,  $V_A$ . The peak absorption wavelength shifts from  $2.7 \mu\text{m}$  to  $2 \mu\text{m}$ . At  $\lambda = 2.1 \mu\text{m}$ , the switching intensity of 75% was observed as shown in Fig. 5. The switching contrast can be calculated as  $SC = (A_{ON} - A_{OFF})/A_{OFF}$ . For the MSCMA devices, the switching contrast was calculated to be 1500%, which is six

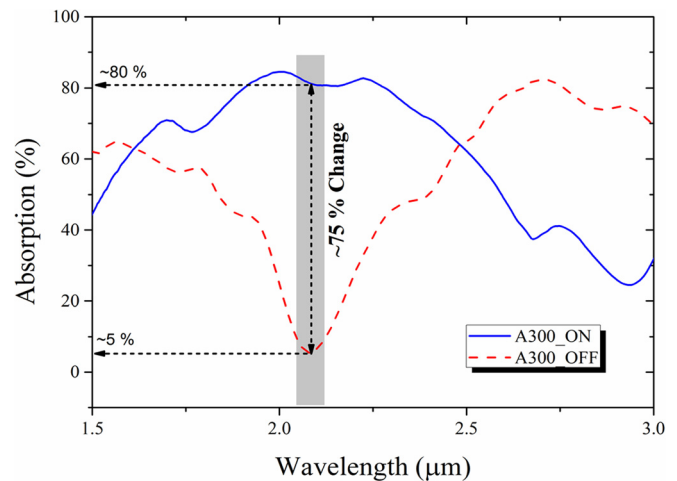


FIG. 5. Electro-optic switching characteristics—Measured absorption spectra of MSCMA with 300 nm air gap in two states—A300\_OFF (Red-dash) and A300\_ON (Blue-solid), respectively.

times higher than 250% contrast in transmission mode in the earlier report using laterally actuated beams in near-IR spectral region.<sup>27</sup>

The proposed MSCMA shows an improved electro-optic performance with simpler design and CMOS compatible fabrication process and materials. The most attractive feature is the integration of metamaterial layer and microactuators as a single entity, and this significantly reduces the overall device footprint. For the external control to tune the metamaterial absorption characteristics, electrostatic potential is used. This can be obtained from application specific ICs (ASICs) that are directly integrated with these devices. Additionally, the material used, i.e., Mo and  $SiO_2$ , is high-temperature stable and is best suited even for rugged environment applications such as space exploration, oil drilling, and mining.<sup>35</sup> Interestingly, as the effective spacer thickness and the peak absorption wavelength are almost linearly related, these devices can also be used for wide range of sensing applications such as accelerometers, pressure sensors, and flow sensors. These devices have a promisingly wide range of application areas with very high potential to be commercialized. However, there is also a lot of room for further improvements, such as process development to achieve stress free suspended CMM Mo layer and precise

patterning of desired CMM pattern shape and size, optimized design for support spring to enable continuously tunable absorber and high frequency modulator applications possible in future.

In summary, a micro-electro-mechanically switchable metamaterial absorber is experimentally demonstrated for near-infrared spectral region using CMOS compatible materials and fabrication process. This technology provides a compact design by integrating the metamaterial layer and out of plane movable microactuators to be a single entity. The devices show a very high switching contrast of 1500% at 2.1  $\mu\text{m}$ . The compact size, high switching contrast, design flexibility, potentially fast response time, and CMOS compatible materials and processes make the reported MEMS switchable metamaterial absorber to be very attractive for mass reproducible devices. These devices can further facilitate numerous optoelectronic applications such as in optical telecommunication, optical signal routers, optical interconnects, multiple gas sensors, and switchable infrared detectors.

The authors acknowledge the financial support from research Grant No. AcRF Tier 2-MOE2012-T2-2-154 at the National University of Singapore.

- <sup>1</sup>R. A. Shelby, D. R. Smith, and S. Schultz, *Science* **292**, 77 (2001).
- <sup>2</sup>J. B. Pendry, D. Schurig, and D. R. Smith, *Science* **312**, 1780 (2006).
- <sup>3</sup>D. Schurig, J. J. Mock, B. J. Justice, S. A. Cummer, J. B. Pendry, A. F. Starr, and D. R. Smith, *Science* **314**, 977 (2006).
- <sup>4</sup>N. Fang, H. Lee, C. Sun, and X. Zhang, *Science* **308**, 534 (2005).
- <sup>5</sup>X. Zhang and Z. Liu, *Nature Mater.* **7**, 435 (2008).
- <sup>6</sup>N. Landy, S. Sajuyigbe, J. Mock, D. Smith, and W. Padilla, *Phys. Rev. Lett.* **100**, 207402 (2008).
- <sup>7</sup>H. Tao, N. I. Landy, C. M. Bingham, X. Zhang, R. D. Averitt, and W. J. Padilla, *Opt. Express* **16**, 7181 (2008).
- <sup>8</sup>N. Liu, M. Mesch, T. Weiss, M. Hentschel, and H. Giessen, *Nano Lett.* **10**, 2342 (2010).
- <sup>9</sup>C. G. Hu, Z. Y. Zhao, X. N. Chen, and X. G. Luo, *Opt. Express* **17**, 16745 (2009).
- <sup>10</sup>C. M. Watts, X. Liu, and W. J. Padilla, *Adv. Mater.* **24**, OP98 (2012).
- <sup>11</sup>H.-T. Chen, J. F. O'Hara, A. K. Azad, A. J. Taylor, R. D. Averitt, D. B. Shrekenhamer, and W. J. Padilla, *Nat. Photonics* **2**, 295 (2008).
- <sup>12</sup>H.-T. Chen, W. J. Padilla, J. M. Zide, A. C. Gossard, A. J. Taylor, and R. D. Averitt, *Nature* **444**, 597 (2006).
- <sup>13</sup>Z. Liu, C. Y. Huang, H. Liu, X. Zhang, and C. Lee, *Opt. Express* **21**, 6519 (2013).
- <sup>14</sup>Y. Y. Jun, H. Y. Jun, W. G. Jun, Z. J. Ping, S. H. Bin, and O. Gordon, *Chin. Phys. B* **21**, 038501 (2012).
- <sup>15</sup>Q. Y. Wen, H. W. Zhang, Q. H. Yang, Z. Chen, Y. Long, Y. L. Jing, Y. Lin, and P. X. Zhang, *J. Phys. D: Appl. Phys.* **45**, 235106 (2012).
- <sup>16</sup>I. M. Pryce, K. Aydin, Y. A. Kelaita, R. M. Briggs, and H. A. Atwater, *Nano Lett.* **10**, 4222 (2010).
- <sup>17</sup>H. Tao, A. C. Strikwerda, K. Fan, W. J. Padilla, X. Zhang, and R. D. Averitt, *Phys. Rev. Lett.* **103**, 147401 (2009).
- <sup>18</sup>J. Y. Ou, E. Plum, L. Jiang, and N. I. Zheludev, *Nano Lett.* **11**, 2142 (2011).
- <sup>19</sup>W. M. Zhu, A. Q. Liu, X. M. Zhang, D. P. Tsai, T. Bourouina, J. H. Teng, X. H. Zhang, H. C. Guo, H. Tanoto, and T. Mei, *Adv. Mater.* **23**, 1792 (2011).
- <sup>20</sup>W. M. Zhu, A. Q. Liu, T. Bourouina, D. P. Tsai, J. H. Teng, X. H. Zhang, G. Q. Lo, D. L. Kwong, and N. I. Zheludev, *Nat. Commun.* **3**, 1274 (2012).
- <sup>21</sup>Y. S. Lin, Y. Qian, F. Ma, Z. Liu, P. Kropelnicki, and C. Lee, *Appl. Phys. Lett.* **102**, 111908 (2013).
- <sup>22</sup>F. Ma, Y. Qian, Y. S. Lin, H. Liu, X. Zhang, Z. Liu, J. M.-L. Tsai, and C. Lee, *Appl. Phys. Lett.* **102**, 161912 (2013).
- <sup>23</sup>Y. S. Lin, F. Ma, and C. Lee, *Opt. Lett.* **38**, 3126 (2013).
- <sup>24</sup>F. Ma, Y. S. Lin, X. Zhang, and C. Lee, *Light: Sci. Appl.* **3**, e171 (2014).
- <sup>25</sup>P. Pitchappa, C. P. Ho, Y. S. Lin, P. Kropelnicki, C. Y. Huang, N. Singh, and C. Lee, *Appl. Phys. Lett.* **104**, 151104 (2014).
- <sup>26</sup>C. P. Ho, P. Pitchappa, Y. S. Lin, C. Y. Huang, P. Kropelnicki, and C. Lee, *Appl. Phys. Lett.* **104**, 161104 (2014).
- <sup>27</sup>J. Y. Ou, E. Plum, J. Zhang, and N. I. Zheludev, *Nat. Nanotechnol.* **8**, 252 (2013).
- <sup>28</sup>H. T. Chen, *Opt. Express* **20**, 7165 (2012).
- <sup>29</sup>J. Kischkat, S. Peters, B. Gruska, M. Semtsiv, M. Chashnikova, M. Klinkmüller, O. Fedosenko, S. Machulik, A. Aleksandrova, G. Monastyrskyi, Y. Flores, and W. T. Masselink, *Appl. Opt.* **51**, 6789 (2012).
- <sup>30</sup>C. P. Ho, P. Pitchappa, P. Kropelnicki, J. Wang, Y. Gu, and C. Lee, *IEEE J. Sel. Top. Quantum Electron.* **20**, 4900107 (2014).
- <sup>31</sup>M. A. Ordal, R. J. Bell, R. W. Alexander, L. L. Long, Jr., and M. R. Querry, *Appl. Opt.* **24**, 4493 (1985).
- <sup>32</sup>H. Y. Zheng, X. R. Jin, J. W. Park, Y. H. Lu, J. Y. Rhee, W. H. Jang, H. Cheong, and Y. P. Lee, *Opt. Express* **20**, 24002 (2012).
- <sup>33</sup>M. Wuttig and N. Yamada, *Nature Mater.* **6**, 824 (2007).
- <sup>34</sup>H. Kind, H. Yan, B. Messer, M. Law, and P. Yang, *Adv. Mater.* **14**, 158 (2002).
- <sup>35</sup>Y. Qian, B. W. Soon, P. Singh, H. Campanella, and C. Lee, *Nanoscale* **6**, 5606 (2014).